High T_c Superconductors: New Insights from Angle-Resolved Photoemission

Mohit Randeria[1] and Juan-Carlos Campuzano[2,3]
(1) Theoretical Physics Group, Tata Institute of Fundamental Research, Mumbai 400005, India
(2) Physics Department, University of Illinois at Chicago, Chicago, IL 60607, USA
(3) Material Science Division, Argonne National Laboratory, Argonne, IL 60439, USA

Abstract

Recent angle-resolved photoemission (ARPES) studies of the high T_c superconductors are reviewed. Amongst the topics discussed are: the spectral function interpretation of ARPES data and sum rules; studies of the momentum distribution and the Fermi surface (FS); dispersion of electronic states, flat bands and superlattice effects; unusual lineshapes and their temperature dependence; the question of bilayer splitting; detailed studies of the superconducting gap and its anisotropy; and, finally, studies of the pseudogap and evolution of the FS with doping in the underdoped materials. [Varenna Lectures, 1997].

Key words: photoemission, high temperature superconductors

1. Introduction

Angle-resolved photoemission spectroscopy (ARPES) [1], [2] is a spectroscopy in which photons are absorbed by the material and electrons are ejected out. The control parameters are the frequency and polarization of the incident photons and the measured quantities are the kinetic energy and the angle of emergence (θ, φ) of the outgoing electron relative to the sample normal.

ARPES is now recognized as one of the major sources of insight into various aspects of the high temperature superconductors (HTSC). This is remarkable, considering that until ten years ago photoemission had never been used as a probe of superconductivity. The first observation of the superconducting gap in angle-integrated PES was given in [3], and in angle-resolved form in [4]. This was followed by the observation of a normal state with a Luttinger Fermi surface [5], [6], flat bands in the dispersion [7], [8], and the anisotropy of the SC gap [9]; see also [10]. In these lectures, we will concentrate on the tremendous progress of the past three years in which, we believe, there has been a qualitative change in thinking about ARPES data and analyzing it. Along with this have come a variety of new physics results which have shed very important new light on the high Tc superconductors.

There are several reasons for the great success of ARPES for the high T_c materials. First, the great improvement in the experimental (especially energy) resolution allows one to study spectral features on the scale of the SC gap in these materials. The FWHM of

the energy resolution is routinely about 20 meV or larger. The large gap energy scales and the higher T_c's help considerably. Second, Bi2212 has a natural cleavage plane in-between the BiO bilayer which is believed to be van der Waals coupled leading to the longest bond length in all the cuprates. This results in extremely smooth surfaces, with minimal charge transfer, which are crucial for ARPES, since this is a surface-sensitive technique due to the short escape depth ($\sim 10\mathring{A}$) of the outgoing electron. The third and final reason is the quasi-two-dimensionality of the electronic structure of the cuprates, which permits one to unambiguously determine the initial state momentum from a final state measurement, since the component of $\mathbf{k}$ parallel to the surface is conserved as the electron emerges from the sample.

Nevertheless, there are important issues which have to be addressed. We have little prior experience in analyzing ARPES data on the energy scale of few 10's of meV. Much of the rest of these lectures will focus on recent efforts towards properly analysing such data, and developing an understanding of low frequency information contained in it. We will focus here on the conceptual issues leaving many of the technical details to the papers referred to in the text.

2. What does ARPES measure?

The theoretical interpretation of ARPES spectra is complicated by the fact that, in general, photoemission measures a *nonlinear* response function. The photo-electron current at the detector is proportional to the number of incident photons, i.e., to the *square* of the vector potential, and the relevant correlation function is a three current correlation, as first emphasized by Shaich and Ashcroft [11].

It is instructive to briefly review their argument. As in standard response function calculations, lets look at an expansion of the current at the detector, the response, in powers of the applied vector potential (incident photons). Let $\mathbf{R}$ be the location of the detector in vacuum, and $\mathbf{r}$ denote points inside the sample. The zeroth order piece $\langle 0|j_\alpha(\mathbf{R},t)|0\rangle$ vanishes as usual; there are no currents flowing anywhere in the absence of the applied field. Here $|0\rangle$ is the ground state of the unperturbed system. The linear response also vanishes. $\langle 0|j_\alpha(\mathbf{R},t)j(\mathbf{r},t')_\beta|0\rangle = 0$ and $\langle 0|j_\alpha(\mathbf{r},t')j_\beta(\mathbf{R},t)|0\rangle = 0$, since there are no particles at the detector, in absence of the e.m. field, and $j_\beta(\mathbf{R},t)|0\rangle = 0$. Thus the leading term which survives is

$$\langle j_\gamma(\mathbf{R},t)\rangle \propto \int d\mathbf{r}'dt'd\mathbf{r}''dt''A_\alpha(\mathbf{r}',t')A_\beta(\mathbf{r}'',t'') \langle 0|j_\alpha(\mathbf{r}',t')j_\gamma(\mathbf{R},t)j_\beta(\mathbf{r}'',t'')|0\rangle \quad (1)$$

where only current operators *inside* the sample act on the unperturbed ground state on either side and the current at the detector is sandwiched in between.

The three current correlation function can be represented by the triangle diagrams [12] of Fig. 1, where the line between the two external photon vertices is the Greens function of the "initial state" or "photo-hole" and the two lines connecting the photon vertex to the current at the detector represent the "photo-electron" which is emitted from the solid. There is a large literature [13] on the ab-initio evaluation of the bare triangle diagram (A), incorporating the realistic electronic structure and surface termination, together with multiple-scattering effects in the photo-electron final state. Such studies are useful for under-

standing the photoemission intensities, but not the line-shape and the many-body aspects of the problem, which are the objects of primary interest for us.

All possible renormalizations – vertex corrections and self energy effects – of the the bare triangle diagram are shown in (B) through (F) of Fig. 1. It is easy to draw these diagrams, but impossible to evaluate them in any controlled calculation! Nevertheless, they are useful in understanding, qualitatively, what the various processes are and in estimating their importance. Diagram (B) represents the many-body renormalization of the occupied initial state that we are interested in; (C) and (D) represent final state line-width broadening and inelastic scattering; (E) is a vertex correction that describes the interaction of the escaping photo-electron with the photo-hole in the solid, and (F) is a vertex correction which combines features of (D) and (E). [An additional issue in a quantitative theory of photoemission is related to the modification of the external vector potential inside the medium, i.e., renormalizations of the photon line.]

Let us first discuss the validity of the sudden approximation, for 15 - 30 eV (ultraviolet) incident photons, by making some simple time scale estimates. The question is: is the outgoing photo-electron sufficiently fast that one can safely ignore its interaction with the photo-hole? The time t spent by the escaping photo-electron in vicinity of photo-hole is the time available for interactions ("vertex corrections") which would invalidate the sudden approximation. A photoelectron with a kinetic energy of (say) 20 eV has a velocity $v = 3 \times 10^8$ cm/s. The relevant length scale, which is the smaller of the screening radius (of the photo-hole) and the escape depth, is $\sim 10\mathring{A}$. Thus $t = 3 \times 10^{-16}$ s. This is to be compared with the time scale for electron-electron interactions (which are the dominant source of interactions at the high frequencies of interest): $t_{ee} \sim 2\pi/\omega_p = 4 \times 10^{-15}$ s, using a plasma frequency $\omega_p \simeq 1$ eV for the cuprates (this would be even lower if c-axis plasmons are involved). *If* $t \ll t_{ee}$, then we can ignore vertex corrections. Our very crude estimate is $t/t_{ee} \simeq 0.1$; all that we can say is that the situation with regard to the validity of the impulse approximation is not hopeless, but clearly a better estimate or a different approach is needed (see below!).

Very similar estimates can be made for renormalizations of the outgoing photo-electron due to its interaction with the medium; again e-e interactions dominate at the energies of interest. The relevant length scale here is the escape depth, which leads to a process of self-selection: those electrons that actually make it to the detector with an appreciable KE have suffered no collisions in the medium. Such estimates indicate that the "inelastic background" must be small – although its precise dependence on $\mathbf{k}$ and ω is uncertain.

To summarize: (1) the corrections to the sudden approximation are probably small and we shall test its validity further below. (2) Final state line-width effects are negligible. A clear experimental proof for Bi2212 is the fact that deep in the SC state a resolution limited spectral peak is seen, as discussed below in Section 6. (3) While the additive extrinsic background due to inelastic scattering is small, its precise form remains an important unresolved problem.

3. Spectral Functions and Sum Rules

Assuming the sudden approximation and ignoring the extrinsic background, the ARPES intensity, or the energy distribution curve (EDC), is given by

$$I(\mathbf{k}, \omega) = I_0(\mathbf{k}) f(\omega) A(\mathbf{k}, \omega) \tag{2}$$

where $\mathbf{k}$, the in-plane momemntum, gives the location in the 2D Brillouin zone, and ω is the energy of the initial state measured relative to the chemical potential. (Experimentally ω is measured relative to the Fermi level of a good metal like Pt or Au in electrical contact with the sample). $I_0(\mathbf{k})$ includes all the kinematical factors and the dipole matrix element (squared). It depends, in addition to $\mathbf{k}$, on the incident photon energy and polarization. The only general constraints on I_0 come from dipole selection rules which we will discuss later on.

The spectral line-shape (ω dependence) of the EDC and its T dependence, at the low frequencies and temperatures of interest to us, are entirely controlled by $f(\omega)A(\mathbf{k},\omega)$. Here $A(\mathbf{k},\omega)$ is the initial state or "photo-hole" spectral function $A(\mathbf{k},\omega) = (-1/\pi)\mathrm{Im}G(\mathbf{k},\omega + i0^+)$, and the the Fermi function $f(\omega) = 1/[\exp(\omega/T) + 1]$ ensures that we are only looking at the *occupied* part of this spectral function. This can formally be seen as follows: the spectral function consists of two pieces $A(\mathbf{k},\omega) = A_+(\mathbf{k},\omega) + A_-(\mathbf{k},\omega)$, which are spectral weights to add and to remove an electron from the system. In ARPES, where one extracts an electron one is measuring $A_-(\mathbf{k},\omega) = \sum_{m,n}\left[e^{-\mathcal{E}_m}/\mathcal{Z}\right]|\langle n|c_{\mathbf{k}}|m\rangle|^2\delta(\omega + \mathcal{E}_n - \mathcal{E}_m)$, which can be rewritten, using standard manipulations, as $A_-(\mathbf{k},\omega) = f(\omega)A(\mathbf{k},\omega)$.

To gain confidence in the validity of a simple spectral function interpretation of ARPES data in the layered cuprates we have used the following strategy [14]. Let us assume that the sudden approximation is valid, deduce some general consequences based on sum rules, and then test those experimentally. The well-known sum rule $\int_{-\infty}^{+\infty} d\omega A(\mathbf{k},\omega) = 1$ is not very useful for ARPES since it is a sum-rule for PES (A_-) *and inverse* PES (A_+). The density of states (DOS) sum rule $\sum_{\mathbf{k}} A(\mathbf{k},\omega) = N(\omega)$ is also not directly useful since there is the $\mathbf{k}$-dependent matrix element factor $I_0(\mathbf{k})$. Very recently, we have looked at the photoemission DOS defined by $N_p(\omega) = \sum_{\mathbf{k}} I_0(\mathbf{k})A(\mathbf{k},\omega)$ in attempt to simulate angle-integrated data by $\mathbf{k}$-summing ARPES data, with very interesting results and strong parallels with STM data; the reader is referred to ref. [15] for this new development.

The important sum rule is

$$\int_{-\infty}^{+\infty} d\omega f(\omega)A(\mathbf{k},\omega) = n(\mathbf{k}), \tag{3}$$

which directly relates the energy-integrated ARPES intensity to the momentum distribution $n(\mathbf{k})$. Somewhat surprisingly its usefulness has never been exploited in the ARPES literature. We will use (3) to derive an approximate sum rule valid at $\mathbf{k}_F$ which we will use to test the validity of the spectral function interpretation and, thereby, (indirectly) of the sudden approximation. Later, having checked this we will use (3) to get experimentally information on $n(\mathbf{k})$.

We first focus on the Fermi surface $\mathbf{k} = \mathbf{k}_F$. One of the major issues that will occupy us in the rest of these lectures, is how to define $\mathbf{k}_F$, at finite temperatures, in a strongly interacting system which may not even have well-defined quasiparticles – and how to to determine it experimentally. At this point, we simply define the Fermi surface to be the $\mathbf{k}$-space locus of gapless excitations in the normal state, so that $A(\mathbf{k}_F,\omega)$ has a peak at $\omega = 0$.

To make further progress with eqn. (3), we need to make a weak particle-hole symmetry assumption: $A(\mathbf{k}_F,-\omega) = A(\mathbf{k}_F,\omega)$ for "small" ω, where "small" means those frequencies for which there is significant T-dependence in the spectral function. It then follows that [14]

$\partial n(\mathbf{k}_F)/\partial T = 0$, i.e., *the integrated area under the EDC at* $\mathbf{k}_F$ *is independent of temperature.* To see this, rewrite eqn. (3) as $n(\mathbf{k}_F) = 1/2 - \int_0^\infty d\omega \tanh(\omega/2T)\left[A(\mathbf{k}_F,\omega) - A(\mathbf{k}_F,-\omega)\right]/2$, and take its T-derivative. It should be emphasized that we cannot say anything about the *value* of $n(\mathbf{k}_F)$, only that it is T-independent. (A much stronger assumption, $A(\mathbf{k}_F,-\omega) = A(\mathbf{k}_F,\omega)$ for *all* ω, is sufficient to give $n(\mathbf{k}_F) = 1/2$ independent of T). We emphasize the approximate nature of the $\mathbf{k}_F$-sum-rule since there is no exact symmetry that enforces it.

We note that we did not make any use of any properties of the spectral function other than the weak p-h symmetry assumption, and to the extent that this is also valid in the SC state, our conclusion $\partial n(\mathbf{k}_F)/\partial T = 0$ holds equally well below T_c. There is the subtle issue of the meaning of "$\mathbf{k}_F$" in the SC state. In analogy with the FS as the "locus of gapless excitations" above T_c, we can define the "minimum gap locus" below T_c. We will describe this in great detail in Section 10 below; it suffices to note here that "$\mathbf{k}_F$" is independent of temperature, within experimental errors, in both the normal and SC state of the systems studied thus far.

4. Experimental Details

We now describe the experiments that first test the above ideas and then use them to get new information. Most of the data to be discussed in these lectures is on very high quality single crystals of $Bi_2Sr_2CaCu_2O_{8+x}$ (Bi2212), grown by the traveling solvent floating zone method with an infrared mirror furnace, with low defect densities and sharp x-ray diffraction rocking curves with structural coherence lengths $\sim 1250\mathring{A}$. The near optimally-doped samples (which we shall focus on, except in the last part of the lectures) have a $T_c = 87$K with a transition width of 1K as determined by a SQUID magnetometer. The samples are cleaved in-situ at 13 K in a vacuum of $< 5\text{x}10^{-11}$ Torr, and have optically flat surfaces as measured by specular laser reflections. Another measure of the sample quality, within ARPES, is the observation of "umklapp" bands in the electronic structure (described below) due to the presence of a structural superlattice distortion.

The experiments were performed at the Synchrotron Radiation Center, Wisconsin, using a high resolution 4-m normal incidence monochromator with a resolving power of 10^4 at 10^{11} photons/s. The samples are carefully oriented in the sample holder to an accuracy 1° by Laue diffraction, and the orientation is further confirmed by the observed symmetry of sharp PES features around high symmetry points. Various experiments have been done using 17 – 22 eV photons, with an energy resolution (FWHM) in the range of 15 – 25 meV and a typical momentum window of angular range $\pm 1^\circ$.

For the Brillouin zone of Bi2212, we use a square lattice notation with the $\Gamma\bar{M}$ along the CuO bond direction. $\Gamma = (0,0)$, $\bar{M} = (\pi,0)$, $X = (\pi,-\pi)$ and $Y = (\pi,\pi)$ in units of $1/a^*$, where $a^* = 3.83\mathring{A}$ is the separation between near neighbor Cu ions. (The orthorhombic a axis is along X and b axis along Y).

5. Experiments on Sum Rule and $n(\mathbf{k})$

Fig. 2(a) shows ARPES spectra for a near-optimal Bi2212 $T_c = 87$ K at the FS crossing along $(\pi,0)$ to (π,π) at two temperatures: $T = 13$ K, which is well below T_c, and $T = 95$ K, which is in the normal state. The two data sets were normalized in the positive energy region [16], which after normalization was chosen to be the common zero baseline. For details, see ref. [14]. Remarkably, even though the spectra themselves are very strongly T-dependent, their integrated intensity in Fig. 2(b) is constant within experimental error

bars (arising from the normalization), as predicted by the $\partial n(\mathbf{k}_F)/\partial T = 0$ sum rule. The sum rule has also been checked at other FS crossings, but is much less informative along the $(0,0)$ to (π,π) crossing where the observed line-shape is not too strongly T-dependent.

An important application of (3) would be to use it to experimentally determine the momentum distribution, particularly since no other methods have successfully addressed this problem for the cuprates (e.g., positron annihilation in $YBa_2Cu_30_7$ apparently only yields information about the chain bands). There are several caveats to keep in mind here, before discussing the data. First, we do not have an absolute scale for the integrated intensity, and, the unknown scale factor is **k**-dependent, since from (2) and (3): $\int d\omega I(\mathbf{k},\omega) = I_0(\mathbf{k})n(\mathbf{k})$. (In principle, electronic structure theory can provide useful input on the **k**-dependence of matrix elements [13]). Second, we do not know what the "zero" for the integrated intensity is, in view of the unknown "extrinsic background". Finally there is the question of the integration limits in (3): while the Fermi function cutoff makes the upper limit irrelevant, the lower limit may be more problematical. Thus, quantitative studies on $n(\mathbf{k})$ are not possible at the moment, but important qualitative information can be extracted as shown below.

In view of the above discussion, we first choose to illustrate the idea of measuring $n(\mathbf{k})$ on $YBa_2Cu_40_8$ (Y124) [7], rather than on Bi2212. The spectra in Fig. 3 (a) and (b) show intense peaks at low energy which get cut off at high binding energies, for the occupied **k** states, and also a loss of emission intensity once $\mathbf{k}_F$ is crossed. Thus the integrated intensity is not seriously affected either by the background problem or uncertainties about the lower limit of integration. The only drawback is the absence of SC within ARPES, presumably due to surface problems, and the Y124 data (bulk $T_c = 82$K) are in a non-superconducting state at 12K. In Fig. 3 (c) and (d), we plot the integrated intensity: the FS crossings along the S-Y-S direction deduced from the dispersion data in (a) are are indicated on the plot in (c). As discussed above, we get information about the momentum distribution to the extent that we assume that the rapid **k**-variation comes from $n(\mathbf{k})$ near the FS, while the prefactor $I_0(\mathbf{k})$ is slowly varying.

The situation in Bi2212 (see Fig. 4) is not as clear cut, both as regards the background, since there is considerable emission after crossing $\mathbf{k}_F$, even though its much smaller than in the occupied states, and as regards the lower limit of integration. Even with these limitations, the integrated intensity shown in Fig. 4 is very informative [17]. (Note that the integrated intensity for **k** way past $\mathbf{k}_F$, i.e. deep on the unoccupied side, is set to zero, by hand). To minimize the effects of the matrix elements and the slowly varying additive background, it is useful to look at peaks in $|\nabla_{\mathbf{k}} n(\mathbf{k})|$. As seen from Fig. 4, these correlate very well with the FS crossing inferred from the dispersion data.

6. ARPES Spectra: Qualitative Features

At this stage, having gained some confidence in interpreting ARPES spectra in terms of the (occupied part of the) one-particle spectral function, let us discuss some of the important qualitative features of the data. The first thing to emphasize is that the peak of the experimental spectrum , the EDC, is *not* necessarily that of the spectral function. This is obvious from eqn. (2), $I \sim f(\omega)A(\mathbf{k},\omega)$, and directly seen from the data in Fig. 5. In the normal state, the EDC peak is produced by the Fermi function $f(\omega)$ cutting off the spectral function $A(\mathbf{k},\omega)$, which would presumably peak at $\omega = 0$ for $\mathbf{k} = \mathbf{k}_F$. We note, in passing,

that recently we have succeeded in developing methods for "dividing out the Fermi function" in the data, which is nontrivial because of the convolution with the energy resolution. This gives very useful direct information about $A(\mathbf{k},\omega)$, as we will discuss elsewhere [15].

An important consequence is that the normal state spectral function is extremely broad, the observed full width of the EDC being less than the actual half-width of $A(\mathbf{k},\omega)$! Does this anomalous normal state spectrum imply a breakdown of Fermi liquid theory, as suggested by numerous transport experiments? In principle, one should be able to answer this question by analyzing the ARPES data using:

$$A(\mathbf{k},\omega) = \frac{\Sigma''(\mathbf{k},\omega)/\pi}{\left(\omega - \epsilon_{\mathbf{k}} - \Sigma'(\mathbf{k},\omega)\right)^2 + \Sigma''(\mathbf{k},\omega)^2} \tag{4}$$

where Σ' and Σ'' are the real and imaginary parts of the self energy. In practice, the number of parameters involved in Σ, coupled with uncertainties about the extrinsic background, lead to serious questions about the uniqueness of such fits. Instead of trying to extract the ω-dependence of Σ it is more useful, at the present time, to focus on the $\mathbf{k}$-dependence of the line-shape as one approaches the FS. For a Fermi liquid, with well defined quasiparticles, the spectrum should sharpen up as $\mathbf{k}_F$ is approached. However, as the normal state data in Fig. 6 clearly show, and simple fits [18] corroborate, this does not happen. *There are no well defined quasiparticles above* T_c! It is very important to emphasize that the large linewidths observed in ARPES are not extrinsic, or artifacts of any analysis. As we will see next, when quasiparticles do exist (for $T \ll T_c$) they are clearly seen in the experiment.

The remarkable T-dependent changes in the line-shape in Figs. 2 and 5 may be understood as follows. For $T < T_c$ the SC gap opens up and spectral weight at $\mathbf{k}_F$ shifts from $\omega = 0$ (in the normal state) to either side of it, of which only the occupied side ($\omega < 0$) is probed by ARPES. At the lowest temperature the EDC peak *is* the peak of the spectral function (unlike the normal state) since, as is obvious from Fig. 5, the fermi function has now become sharper and spectral weight has moved down to below the gap energy. A detailed analysis of the SC gap data will described in Section 10 below.

Another striking feature of the data is the sharpening of the peak with decreasing T in the SC state. This is *not* a "BCS pile up" in the density of states, a description frequently used in the early literature, since we are not measuring a DOS. With a rapid decrease in linewidth below T_c, the only way the conserved area sum rule can be satisfied is by having a large rise in intensity. The dramatic decrease in the linewidth (Σ'') below T_c is a consequence of the the SC gap leading to a suppression of electron-electron scattering which was responsible for the large linewidth above T_c. *Thus coherent quasiparticle (q.p.) excitations do exist for* $T \ll T_c$ [19]. The rapid T-dependence of the line width is in qualitative agreement with the results of various transport measurements [20]. A quantitative extraction of the scattering rate from ARPES data is an important open problem.

It is worth emphasizing that every aspect of this data, from the broad normal state spectrum to the highly non-trivial SC state line shape, points to the importance of e-e interactions. The strong T-dependence of the linewidth is very unusual, and would not occur in conventional metallic SC's where the e-e interaction contribution to the scattering rate is weak. We will argue below that e-e interactions are also responsible for the non-trivial dip and hump structure (see Fig. 2) present beyond the sharp q.p. peak in the SC state; see

Section 9. Finally, the fact that we see spectral shifts in the same data all the way down to 100 meV $\sim$ 1000 K, for a temperature change of 100 K, also suggests that e-e interactions are at work.

7. Normal State of Optimally Doped Bi2212

We now briefly summarize the main results of a very detailed study [21] of the electronic excitations in the normal state (T = 95K) of near-optimal Bi2212 (T_c = 87K). We begin with a discussion of the dispersion of the electronic excitations and the Fermi Surface. Two representative data sets are plotted in Fig. 6: the left panel shows dispersing peaks along the diagonal $(0,0)$ to (π,π), while the right panel shows data along the zone boundary $(\pi,0)$ to $(\pi,-\pi)$. Spectral peak positions as a function of $\mathbf{k}$ are plotted in Fig. 7(b), and the corresponding Fermi surface (FS) crossings in Fig. 7(a).

In addition to the symbols in Fig. 7, there are also several curves, which we now describe; these curves make clear the significance of all of the observed features. The thick curve is a 6-parameter tight-binding fit [22] to the Y-quadrant data; this represents the main CuO_2 band. The two thin curves are obtained by shifting the main band fit by $\pm\mathbf{Q}$ respectively, where $\mathbf{Q} = (0.21\pi, 0.21\pi)$ is the superlattice (SL) vector known from structural studies [23]. We also have a few data points lying on a dashed curve, which is obtained by shifting the $\mathbf{k}$ of the main band by (π,π); this "shadow band" will be discussed below. The Fermi surfaces corresponding to the main band fit (thick line), the SL umklapps (thin lines) and the shadow band (dashed) are are plotted as curves in Fig. 7(a). We note that the main FS is a large hole-like barrel centered about the (π,π) point whose enclosed area corresponds to approximately 1.17 holes per planar Cu (i.e., a hole doping of 0.17). One of the key questions is why only one CuO main band is found in Bi2212 which is a bilayer material. We will discuss this in depth in the Section 9.

The next important point relates to the "shadow bands" first observed in ARPES experiments [24] done in a rather different mode (roughly, those experiments measure $\int_{\delta\omega} d\omega A(\mathbf{k},\omega)$ over a small range $\delta\omega$ near $\omega = 0$). The shadow bands were not seen earlier in the EDC mode experiments probably because of their sensitive photon energy dependence and the absence of a strong feature near E_F. These "shadow bands" were predicted early on to arise from short ranged antiferromagnetic correlations [25]. An alternative explanation, which needs to be tested further, is that they are of structural origin: Bi2212 has a face-centered orthorhombic cell with two inequivalent Cu sites per plane, which by itself could generate a (π,π) umklapp.

We now turn to the effect of the superlattice (SL) on the ARPES spectra. This is very important, since a lack of understanding of these effects led to incorrect conclusions regarding such basic issues as one versus two Femi surfaces (see Section 9), and the anisotropy of the SC gap (see Section 10). All of the experimental evidence is in favour of interpreting the SL umklapp bands as arising from a final state effect in which the exiting photo-electron scatters off the structural SL superlattice distortion (which lives primarily) on the Bi-O layer [26].

We use the polarization selection rules to disentangle the main and SL bands in the X-quadrant where the main and umklapp FSs are very close together; see Fig. 7(a). The point is that ΓX (together with the z-axis) and, similarly ΓY, are mirror planes, and an initial state arising from an orbital which has $d_{x^2-y^2}$ symmetry about a planar Cu-site is odd

under reflection in these mirror planes. With the detector placed in the mirror plane the final state is even, and one expects a dipole-allowed transition when the photon polarization **A** is perpendicular to (odd about) the mirror plane, but no emission when the polarization is parallel to (even about) the mirror plane. While this selection rule is obeyed along ΓY it is violated along ΓX. In fact this apparent violation of selection rules in the X quadrant, was a puzzling feature of all previous studies [10] of Bi2212. It was first pointed out in ref. [27], and then experimentally verified in ref. [21], that this "forbidden" $\Gamma X||$ emission originates from the SL umklapps. We will come back to the $\Gamma X||$ emission in the superconducting state below.

8. Extended Saddle Point Singularity

Some aspects of the normal state dispersion plotted in Fig. 7(b) deserve special mention: while the dispersion along the diagonal $(0,0)$ to (π,π) is very rapid, that near the $(\pi,0)$ point is very flat. In particular, along $(0,0)$ to $(\pi,0)$ there is an intense spectral peak is the main band, which disperses towards E_F but stays just below it at a binding energy of (approximately) -30 meV. This is often called the "flat band" or "extended saddle point", and appears to exist in all cuprates, though at different binding energies in different materials [7], [8], [10].

In our opinion this flat band is not a consequence of the bare electronic structure but rather a many-body effect. The argument for this is that a tight-binding description of such a dispersion requires fine-tuning (of the ratio of the next-near neighbour hopping to the near-neighbour hopping) which would be unnatural even in one material, let alone many.

Another important issue is whether this flat band leads to a singular density of states. It is very important to recognize that, while Fig. 7 (b) *looks like* a conventional band structure, the dispersing states whose "centroids" or "peak positions" are plotted are extremely broad, with width comparable to binding energy, and these simply cannot be thought of as quasiparticles. This general point is true at all $\mathbf{k}$'s, but specifically for the flat band region it has the effect of spreading out the spectral weight over such a broad range that any singularity in the DOS would be washed out.

9. Bilayer Splitting?

On very general grounds, one expects that the two CuO_2 layers in a unit cell of Bi2212 should hybridize to produce two electronic states which are even and odd under reflection in a mirror plane mid-way between the layers. Where are these two states? Why did we find only one main "band" and only one FS in Fig.7?

We have carefully checked the absence of a FS crossing for the main band along $\Gamma\bar{M}$ by studying the integrated intensity and its derivative $|\nabla_{\mathbf{k}} n(\mathbf{k})|$ and found no sharp feature in $n(\mathbf{k})$. Further the FS crossing that we do see near $(\pi,0)$ along $\Gamma\bar{M}$ in Fig.7(a) is clearly associated with a SL umklapp band, as seen both from the dispersion data in Fig.7 (b) and its polarization analysis. This FS crossing is only seen in the $\Gamma\bar{M}$ $\perp$ (odd) geometry both in our data and in earlier work [8] (where it was erroneously identified as part of a second FS closed round around Γ). Emission from the main $d_{x^2-y^2}$ band, which is even about $\Gamma\bar{M}$, is dipole forbidden, and one only observes a weak SL signal crossing E_F. This clearly demonstrates that the bilayer splitting of the CuO_2 states does not lead to two experimentally resolvable Fermi surfaces.

It should be emphasized that this, by itself, is not in contradiction with electronic struc-

ture calculations [28]. Whether or not the two Fermi surfaces are resolvable depends sensitively on the exact doping levels and on the presence of Bi-O pockets, which are neither treated accurately in the theory nor observed in the ARPES data. However, there *is* a clear prediction from band theory: at $\bar{M} = (\pi, 0)$, where both states are occupied the bilayer splitting is the largest, of order 0.25 eV.

The normal state spectrum at $\bar{M}$ is so broad that it may be hard to resolve two states. However, for $T \ll T_c$, when a sharp quasiparticle peak is seen, the bilayer splitting should be readily observable. For this one needs to interpret the non-trivial line shape at $\bar{M}$ shown in Fig. 8: with a dip [10], [29] in between the q.p. peak and a broad bump at 100 meV. Probably the simplest interpretation would be (I) where the bump is the second band, which is resolved below T_c once the first band becomes sharp. The other alternative (II) is that non-trivial line shape is due to many-body effects in a single spectral function $A(\mathbf{k}, \omega)$. To choose between these two hypotheses, we exploit the polarization dependence of the matrix elements. In case (I) there are two independent matrix elements which, in general, should vary differently with $\mathbf{A}$, and thus the intensities of the two features should vary independently. While for case (II), the intensities of the two features should scale together. In ref. [21] we found, by varying the z-component of $\mathbf{A}$, evidence supporting hypothesis (II): the q.p. peak, dip and bump are all part of a single spectral function for Bi2212. The same conclusion can be quite independently reached from the dispersion data in the SC and normal states shown in ref. [30]. Additional experimental evidence against a two band interpretation of the dip structure comes from tunneling [31].

There are two important questions arising from this conclusion. First, what causes this non-trivial line shape? The answer is the non-trivial ω-dependence of the self energy: at low ω, Σ'' is suppressed by the opening of the gap which leads to the q.p. peak, but at $\omega \gg \Delta$, Σ must recover its normal state behavior. This effect is qualitatively able to account for the dip-bump structure [32]. A more quantitative description of the SC line-shape is lacking at the present time; for some recent progress in this direction, see [30].

The second question to ask is: what conspires to keep the two states degenerate? Anderson [33] had predicted that many-body effects within a single layer would destroy both the quasiparticles and the coherent bilayer splitting *in the normal state*. But why the splitting should not be visible in the SC state, where q.p.'s do exist, is not so clear. Finally, it should be mentioned that, in contrast to the Bi2212 case, there is some evidence for bilayer-split bands in YBCO [5], [34], [7], although this problem needs further investigation.

10. Superconducting Gap and its Anisotropy

In this Section, we will first establish how the SC gap manifests itself in ARPES spectra, and then directly map out its variation with $\mathbf{k}$ along the FS. Since ARPES is the only available technique for obtaining such information, it has a played an important role [9], [35] in establishing the d-wave order parameter in the high Tc superconductors [36].

In Fig. 9 we show SC state spectra for Bi2212 for a sequence of $\mathbf{k}$'s. In the normal state these $\mathbf{k}$'s go from the occupied (top) to unoccupied (bottom) states, through $\mathbf{k}_F$, as shown in Fig. 4. However, in the SC state the spectral peaks do not disperse through the chemical potential, rather they first approach $\omega = 0$ and then recede away from it, as can be clearly seen from Fig. 9 (b). In comparing the normal and SC state data in Figs. 4 and 9 (which have different energy scales!), it is important to bear in mind the discussion in Section 6

based on Fig. 5 that in the normal state the EDC peak is caused by the Fermi function cut-off while for a gapped spectrum, the EDC peak is that of the spectral function.

There are several important conclusions to be drawn from Fig. 9. First the bending back of the spectral peak, for $\mathbf{k}$ beyond $\mathbf{k}_F$, is direct evidence for particle-hole mixing in the SC state; for details see ref. [17]. The energy of closest approach to $\omega = 0$ is related to the SC gap that has opened up at the FS, and a quantitative estimate of this gap will be described below. The location of closest approach to $\omega = 0$ ("minimum gap") coincides, within experimental uncertainties, with the $\mathbf{k}_F$ obtained from the normal state $n(\mathbf{k})$ analysis of Fig. 4. It is important for later purposes to note that the "minimum gap locus", determined in this way, gives information about the underlying FS (which is, of course, gapped below T_c).

In Fig. 10, we show the $T = 13$K EDCs for the 87K T_c sample for various points on the main band FS in the Y-quadrant. Each spectrum shown corresponds to the minimum observable gap along a set of $\mathbf{k}$ points normal to the FS, obtained from a dense sampling of $\mathbf{k}$-space [37]. We used 22 eV photons in a ΓY $\perp$ polarization, with a 17 meV (FWHM) energy resolution, and a $\mathbf{k}$-window of radius $0.045\pi/a^*$.

The simplest gap estimate is obtained from the mid-point shift of the leading edge of Bi2212 relative to Pt in electrical contact with the sample. This has no obvious quantitative validity, since the Bi2212 EDC is a spectral function while the polycrystalline Pt spectrum (dashed curve in Fig. 10) is a weighted density of states whose leading edge is an energy-resolution limited Fermi function. We see that the shifts (open circles in Fig. 11) indicate a highly anisotropic gap which vanishes in the nodal directions, and these results are qualitatively similar to ones obtained from the fits described below.

Next we turn to modeling [35], [38] the SC state data in terms of spectral functions. It is important to ask how can we model the non-trivial line shape (with the dip-bump structure at high ω) in the absence of a detailed theory, and, second, how do we deal with the extrinsic background? We argue as follows: in the large gap region near $(\pi, 0)$, we see a linewidth collapse for frequencies smaller than $\sim 3\Delta$ upon cooling well below T_c. Thus for estimating the SC gap at the low temperature, it is sufficient to look at small frequencies, and to focus on the coherent (resolution limited) piece of the spectral function. (Note this argument fails at higher temperatures, e.g., just below T_c). We model this coherent piece by the BCS spectral function $A(\mathbf{k},\omega) = u_{\mathbf{k}}^2\Gamma/\pi\,[(\omega - E_{\mathbf{k}})^2 + \Gamma^2] + v_{\mathbf{k}}^2\Gamma/\pi\,[(\omega + E_{\mathbf{k}})^2 + \Gamma^2]$ where the coherence factors are $v_{\mathbf{k}}^2 = 1 - u_{\mathbf{k}}^2 = \frac{1}{2}(1 - \epsilon_{\mathbf{k}}/E_{\mathbf{k}})$ and Γ is a phenomenological linewidth. The normal state energy $\epsilon_{\mathbf{k}}$ is measured from E_F and the Bogoliubov quasiparticle energy is $E_{\mathbf{k}} = \sqrt{\epsilon_{\mathbf{k}}^2 + |\Delta(\mathbf{k})|^2}$, where $\Delta(\mathbf{k})$ is the gap function. Note that only the second term in $A(\mathbf{k},\omega)$, with the $v_{\mathbf{k}}^2$-coefficient, makes a significant contribution to the ARPES spectra.

The effects of experimental resolution are taken into account via

$$\tilde{I}(\mathbf{k},\omega) = I_0 \int_{\delta\mathbf{k}} d\mathbf{k}' \int_{-\infty}^{+\infty} d\omega' R(\omega - \omega') f(\omega') A(\mathbf{k}',\omega') \tag{5}$$

where $R(\omega)$, the energy resolution, is a normalized Gausian and $\delta\mathbf{k}$ is the $\mathbf{k}$-window of the analyzer. In so far as the fitting procedure is concerned, all of the incoherent part of the spectral function is lumped together with the experimental background into one function which is added to the $\tilde{I}$ above. Since the gap is determined by fitting the resolution-limited leading edge of the EDC, its value is insensitive to this drastic simplification. To check this,

we have made an independent set of fits where we do not use any background fitting function, and only try to match the leading edges, not the full spectrum. The two gap estimates are consistent within a meV. Once the insensitivity of the gap to the assumed background is established, there are only two free parameters in the fit at each $\mathbf{k}$: the overall intensity I_0 and the gap $|\Delta|$; the dispersion $\epsilon_{\mathbf{k}}$ is known from the normal state study, the small linewidth Γ is dominated by the resolution.

The other important question is the justification for using a coherent spectral function to model the rather broad EDC along and near the diagonal direction. We have found that such a description is self-consistent [35], [38] (though perhaps not unique), with the entire width of the EDC accounted for by the large dispersion (of about 60 meV within our $\mathbf{k}$-window) along the zone diagonal.

The gaps extracted from fits to the spectra of Fig. 10 are shown as filled symbols in Fig. 11. For a detailed discussion of the the error bars and also of sample-to-sample variations we refer the reader to ref. [35]. The angular variation of the gap obtained from the fits is in excellent agreement with $|\cos(k_x) - \cos(k_y)|$ form. The ARPES experiment cannot of course measure the phase of the order parameter, but this result is strongly suggestive of $d_{x^2-y^2}$ pairing. Such an order parameter arises naturally in theories with strong correlations and/or antiferromagnetic spin fluctuations [39].

For completeness, we add few lines clarifying the earlier observation of two nodes in the X-quadrant [38], and the related non-zero gap along ΓX in the $\Gamma X||$ geometry [38], [40]. It was realized soon afterwards that these observations were related to gaps on the superlattice bands [27], and not on the main band. To prove this experimentally, the X-quadrant gap has been studied in the $\Gamma X \perp$ geometry [35] and found to be consistent with Y-quadrant $d_{x^2-y^2}$ result described above.

11. Pseudogap in the underdoped materials

We finally turn to one of the most fascinating recent developments – pseudogaps – in high T_c superconductors in which ARPES has again played a major role [41], [42], [43]. Our discussion here will be rather brief as pseudogaps will be the main topic of a companion set of lectures by one of us (M.R.), where the reader will also find more detailed references on the comparison of ARPES with other probes of the pseudogap, and of various theoretical approaches [44].

Up to this point we have discussed optimally doped Bi2212. We now contrast this with the remarkable behaviour of the underdoped materials, where T_c is suppressed by lowering the carrier (hole) concentration. See Fig. 12 for a schematic phase diagram [41]. Underdoping was achieved by adjusting the oxygen partial pressure during annealing the float-zone grown crystals. These crystals also have structural coherence lengths of at least 1,250$\mathring{A}$ as seen from x-ray diffraction, and optically flat surfaces upon cleaving, similar to the near-optimally doped T_c samples discussed above. (Actually, those samples are now believed to be slightly overdopded, optimal doping corresponding to $T_c = 92$K). We denote the underdoped samples by their onset T_c: the 83K sample has a transition width of 2K and the highly underdoped 15K and 10K have transition widths > 5K. (Other groups have also studied samples where underdoping was achieved by cation substitution [42]).

The first point to note about the high temperature ARPES spectra of underdoped Bi2212 is that they become progressively broader with underdoping. While the excitations of the

optimally doped material were anomalously broad (non-Fermi liquid behaviour), there was nevertheless an identifiable spectral peak in the normal state. In contrast, the underdoped spectra above T_c are so broad that there is no identifiable peak at all. One might question: how do we know that these featureless EDCs are spectral functions? There are two reasons: first, even above T_c there is observable dispersion, and second, way below T_c a coherent (almost resolution-limited) quasi-particle peak emerges (in the 83K T_c samples in which this regime is accessible).

In fact the SC state spectra in the underdoped regime look very similar to those at optimal doping, with the one difference that the spectral weight in the coherent q.p. peak diminishes rapidly with underdoping. It is not possible at the present time to quantify this important observation. The "minimum gap locus" in the SC state (see Section 10) suggests a large underlying Fermi surface, satisfying the Luttinger count of count of $(1 + x)$ holes per planar Cu, and coincides with the high temperature FS, which is the locus of gapless excitations [43]. The SC gap is found to be highly anisotropic, with a node along the diagonal, and its **k** variation along the FS is consistent with that of the optimally doped sample; see Fig. 13(a).

The major difference with the optimally doped sample is evident upon heating through T_c. While the gapless excitations along the diagonal remain gapless, the large gap along the $(\pi, 0)$ to (π, π) crossing does not close above T_c, as seen from Fig. 13(b). One has to go to a (crossover scale) T^* which is much higher than T_c before this gap vanishes and a closed contour of gapless excitations (the FS) is recovered. Note that in Fig. 13 we use the leading edge shift to estimate the gap, since except for $T \ll T_c$ we do not know enough about the line-shape to make any quantitative fits (as explained in Section 10).

It is important to emphasize that our understanding of the 83K T_c sample is the best amongst all the underdoped materials. In this sample all three regimes – the SC state below T_c, the pseudogap regime (83K= $T_c < T < T^*$=170K) and the gapless "normal" regime above T^* – have been studied in detail. In contrast, the 10K and 15K samples have such low T_c's and such high T^*'s that only the pseudogap regime is experimentally accessible. Nevertheless, the results on the heavily underdoped samples appear to be a natural continuation of the weakly underdoped materials and the results (similar, perhaps slightly larger [45], magnitude of gap, higher value of T^*) on the low T_c samples are in qualitative agreement with those obtained from other probes (see ref. [44]). Perhaps the most controversial of the results on the heavily underdoped samples is the inference about a large underlying FS from the "minimum gap locus" in the pseudogap regime [43] as opposed to small hole pockets. While this is certainly a tricky issue, and there may also be materials problems in the very low T_c sample, we did not find any evidence for either the closure of a hole pocket (concave arc about the Γ point) or for shadow bands which are (π, π)-foldbacks of the observed state.

To summarize the ARPES results in the underdoped regime: a highly anisotropic SC gap is found in the underdoped samples which is essentially independent of the doping level both in its magnitude [45] and in its **k**-dependence. Thus in this respect the underdoped samples are very similar to optimally doped Bi2212. The key differences in the SC state are first, the value of T_c, and second, the spectral weight in the coherent q.p. peak at $T \ll T_c$, both of which drop rapidly with underdoping. Above T_c the ARPES spectra in the underdoped state are qualitatively different from optimal doping. ARPES continues to show a gap which

evolves smoothly through T_c and has essentially the same anisotropy as the SC gap. This suppression of spectral weight, called the pseudogap, persists all the way to a much higher scale T^* at which a locus of gapless excitations (Fermi surface) is recovered.

12. Conclusions

In conclusion, we hope that we have been able to convey to the readers the exciting new physics that has come out of ARPES studies of the high T_c superconductors. What is really astonishing is the range of issues on which ARPES has given new insights: from non-Fermi liquid behaviour with a Fermi surface, to the symmetry of the order parameter, to the development of a Fermi surface in a doped Mott-insulator and the pseudo-gap phenomena in the underdoped cuprates.

Acknowledgements

We gratefully acknowledge the contribution of all our collaborators, and would particularly like to thank Hong Ding and Mike Norman for the countless discussions which have shaped our understanding of the issues involved. JCC was supported by the U. S. Dept. of Energy, Basic Energy Sciences, under contract W-31-109-ENG-38, the National Science Foundation DMR 9624048, and DMR 91-20000 through the Science and Technology Center for Superconductivity.

REFERENCES

[1] S. Hüfner, *Photoelectron Spectroscopy*, (Springer Verlag, Berlin, 1995).

[2] *Photoemission in Solids* I, edited by M. Cardona and L. Ley, (Springer Verlag, Berlin, 1978).

[3] J-M. Imer *et al.*, Phys. Rev. Lett. **62**, 336 (1989).

[4] C.G. Olson *et al.*, Science **245**, 731 (1989).

[5] J. C. Campuzano *et al.*, Phys. Rev. Lett. **64**, 2308 (1990).

[6] C.G. Olson *et al.*, Phys. Rev. B**42**, 381 (1990).

[7] K. Gofron *et al.*, J. Phys. Chem. Sol. **54**, 1193 (1993) and Phys. Rev. Lett. **73**, 3302 (1994).

[8] D. S. Dessau *et al.*, Phys. Rev. Lett. **71**, 2781 (1993).

[9] Z. X. Shen *et al.*, Phys. Rev. Lett. **70**, 1553 (1993).

[10] For a review of the first five years of work on the cuprates, see Sec. 4 and 5 of Z. X. Shen and D. S. Dessau, Phys. Repts. **253**, 1 (1995).

[11] W. L. Shaich and N. W. Ashcroft, Phys. Rev. **B 3**, 2452 (1971).

[12] C. Caroli, D. Lederer-Rozenblatt, B. Roulet, and D. Saint-James, Phys. Rev. **B 8**, 4552 (1973).

[13] R. Pendry, Surf. Sci. **57**, 679 (1976). For a review of applications of these methods to the cuprates, see: A. Bansil and M. Lindroos, J. Phys. Chem. Solids **56**, 1855 (1995).

[14] M. Randeria, H. Ding, J. C. Campuzano, A. Bellman, G. Jennings, T. Yokoya, T. Takahashi, H. Katayama-Yoshida, T. Mochiku, and K. Kadowaki, Phys. Rev. Lett. **74**, 4591 (1995).

[15] Work in progress with M.R. Norman and H. Ding.

[16] The essentially ω-independent emission at positive frequencies, which is not cut-off by the Fermi function, is due to higher harmonics of the incident photon beam ("second order light").

[17] J. C. Campuzano, H. Ding, M. R. Norman, M. Randeria, A. Bellman, T. Yokoya, T. Takahashi, H. Katayama-Yoshida, T. Mochiku, K. Kadowaki, and G. Jennings, *Phys. Rev.* **B 53** R14737, (1996).

[18] We have found that simple ways of analyzing the data are adequate to establish this, unlike the low frequency behavior of the self energy. Ding *et al.*(unpublished).

[19] Actually, this has been established only for $\mathbf{k}$'s around $(\pi, 0)$. We cannot answer the question of whether quasiparticles exist for $T \ll T_c$ along the $(0, 0)$ to (π, π) FS crossing because of the rapid dispersion within our $\mathbf{k}$-window (see Fig. 7 and also Section 10).

[20] M. C. Nuss *et al.*, Phys. Rev. Lett. **66**, 3305 (1991); W.N. Hardy *et al.*, Phys. Rev. Lett. **70**, 399 (1993); K. Krishana, J.M. Harris, and N.P. Ong, Phys. Rev. Lett. **75**, 3529 (1995).

[21] H. Ding, A. Bellman, J. C. Campuzano, M. Randeria, M. R. Norman, T. Yokoya, T. Takahashi, H. Katayama-Yoshida, T. Mochiku, K. Kadowaki, G. Jennings, and G. P. Brivio, *Phys. Rev. Lett.* **B 76**, 1533 (1996).

[22] M. R. Norman, M. Randeria, H. Ding, and J. C. Campuzano, Phys. Rev. **B 52**, 615 (1995).

[23] R. L. Withers *et al.*, J. Phys. **C 21**, 6067 (1988).

[24] P. Aebi *et al.*, Phys. Rev. Lett. **72**, 2757 (1994).

[25] A. Kampf and J. R. Schrieffer, Phys. Rev. **B 42**, 7967 (1990).

[26] This would allow us to understand (1) why polarization selection rules are obeyed for the $\Gamma\bar{M}$ mirror plane, and (2) qualitatively, why the intensities for odd (only main-band contributes) and even (only the SL contributes) polarizations along ΓX are comparable. This point was not fully appreciated at the time [21] was published

[27] M. R. Norman, M. Randeria, H. Ding, J. C. Campuzano, and A. F. Bellman, *Phys. Rev.* **B 52**, 15107 (1995).

[28] S. Massida, J. Yu, and A.J. Freeman, Physica **C 152**, 251 (1988); O. K. Andersen *et al.*, Phys. Rev. **B 49**, 4145 (1994).

[29] D.S. Dessau *et al.*, Phys. Rev. Lett. **66**, 2160 (1991).

[30] M. R. Norman, H. Ding, J. C. Campuzano, T. Takeuchi, M. Randeria, T. Yokoya, T. Takahashi, T. Mochiku, and K. Kadowaki cond-mat/9702144 and Phys. Rev. Lett. (1997), to appear.

[31] There is striking evidence in point-contact tunneling data on a variety of cuprates (including some one-layer per unit cell materials) that the dip-hump structure scales with the gap; see J. Zasadzinski *et al.* (unpublished) in Fig. 1 of D. Coffey, J. Phys. Chem. Solids **54**, 1369 (1993).

[32] C. M. Varma and P. B. Littlewood, Phys. Rev. **B 46**, 405 (1992); L. Coffey and D. Coffey, Phys. Rev. **B 48**, 4184 (1993).

[33] P. W. Anderson, Science **256**, 1526 (1992).

[34] R. Liu *et al.*, Phys. Rev. **B45**, 5614 (1992) and **B46**, 11056 (1992).

[35] H. Ding, M. R. Norman, J. C. Campuzano, M. Randeria, A. Bellman, T. Yokoya, T. Takahashi, T. Mochiku, and K. Kadowaki, *Phys. Rev.* **B 54** R9678 (1996).

[36] B. Goss-Levi, Physics Today, **49**, 1, p. 19 (1996).

[37] The large dispersion along ΓY, of about 60 meV within our momentum window $\delta\mathbf{k}$, makes it hard to locate $\mathbf{k}_F$ accurately and to map out the nodal region. To this end the we use a step size of $\delta\mathbf{k}/2$ normal to the FS and $\delta\mathbf{k}$ along it.

[38] H. Ding, J. C. Campuzano, A. Bellman, T. Yokoya, M. R. Norman, M. Randeria, T. Takahashi, H. Katayama-Yoshida, T. Mochiku, K. Kadowaki, and G. Jennings, Phys. Rev. Lett. **74**, 2784 (1995) and **75**, 1425(E) (1995).

[39] See: D. Pines and P. Monthoux, J. Phys. Chem. Solids **56**, 1651 (1995) and D. J. Scalapino, Phys. Rep. **250**, 329 (1995).

[40] R. J. Kelley et al., Phys. Rev. B **50**, 590 (1994).

[41] H. Ding, T. Yokoya, J.C. Campuzano, T. Takahashi, M. Randeria, M.R. Norman, T. Mochiku, K. Kadowaki, and J. Giapintzakis, Nature **382**, 51 (1996).

[42] D.S. Marshall *et al*, Phys. Rev. Lett. **76**, 4841 (1996). A. Loesser *et al*, Science, bf 273, 325 (1996).

[43] H. Ding, M.R. Norman, T. Yokoya, T. Takuechi, M. Randeria, J.C. Campuzano, T. Takahashi, T. Mochiku, and K. Kadowaki, Phys. Rev. Lett. **78**, 2628 (1997).

[44] M. Randeria, Varenna Lectures on "Precursor Pairing Correlations and Pseudogaps" (1997).

[45] Recent data clearly shows that, inspite of some sample-to-sample variation, there is a systematic trend for the maximum SC gap to increase with increasing underdoping.

FIGURES

FIG. 1. Diagrams contributing to the three-current correlation formulation of the ARPES intensity. The dark lines are renormalized propagators and the shaded blocks are vertex corrections. For simplicity the arrows are shown in only (A). The physical processes represented by each diagram are discussed in the text.

FIG. 2. (a) ARPES spectra for Bi2212 $T_c = 87$ K at $\mathbf{k} = \mathbf{k}_F$ (FS crossing along $(\pi, 0)$ to (π, π)) at $T = 13$ K and $T = 95$ K. (b) Integrated intensity vs. temperature showing that the area is conserved.

FIG. 3. (a) and (b): EDCs for $YBa_2Cu_40_8$ at 12 K for various $\mathbf{k}$'s. Spectra labeled 1 through 13 are along the SYS direction and spectra 14 though 18 are along ΓY. (c) and (d): Integrated intensity, proportional to $n(\mathbf{k})$, for the EDCs in (a) and (b). The $\mathbf{k}$ points are indicated in the BZ, the hatched area denotes occupied states. The arrows show Fermi surface crossings inferred from the dispersion. The $\mathbf{k}$-resolution of ± 1 degree corresponds to $\delta k_x a \simeq \pm 0.17$ as shown.

FIG. 4. (a): Normal state ($T = 95$K) Bi2212 spectra for a set of $\mathbf{k}$ values (in units of $1/a^*$). (b): Integrated intensity (black dots) from data in (a) giving information about the momentum distribution; its derivative is shown by a solid curve (arbitrary scale).

FIG. 5. SC ($T = 13$K) and normal state ($T = 95$K) Bi2212 spectra (solid curves) and reference Pt spectra (dashed curves) at the same temperatures. This shows how the fermi function cutoff produces the normal state EDC peak, but the peak in the SC state is an intrinsic feature of the spectral function.

FIG. 6. Normal state (T=95K) spectra for Bi2212 along two symmetry lines at values of the momenta shown as open circles in the upper insets. The photon polarization, $\mathbf{A}$, is horizontonal in each panel.

FIG. 7. Fermi surface (a) and dispersion (b) obtained from normal state measurements. The thick lines are obtained by a tight binding fit to the dispersion data of the main band with the thin lines $(0.21\pi, 0.21\pi)$ umklapps and the dashed lines (π, π) umklapps of the main band. Open circles in (a) are the data. In (b), filled circles are for odd initial states (relative to the corresponding mirror plane), open circles for even initial states, and triangles for data taken in a mixed geometry. The inset of (b) is a blowup of ΓX.

FIG. 8. Low temperature (T=13K) EDC's of Bi2212 at $\bar{M}$ for various incident photon angles. The solid (dashed) line is 18° (85°) from the normal. The inset shows the height of the sharp peak for data normalized to the broad bump, at different incident angles.

FIG. 9. Superconducting state EDCs for Bi2212 for the set of **k**-values (1/a units) which are shown at the top. (For corresponding normal state data, see Fig. 4). (b) SC state peak positions (white dots) versus **k** for data of part (a). The $\mathbf{k}_F$ marked is the same as that determined from the normal state analysis of Fig. 4.

FIG. 10. Bi2212 spectra (solid lines) for a 87K T_c sample at 13K and Pt spectra (dashed lines) versus binding energy (meV) along the Fermi surface in the Y quadrant. The photon polarization and BZ locations of the data points are shown in inset to Fig 11.

FIG. 11. Y quadrant gap in meV versus angle on the Fermi surface (filled circles) from fits to the data of Fig. 10. Open symbols show leading edge shift with respect to Pt reference. The solid curve is a d-wave fits to the filled symbols.

FIG. 12. Schematic phase diagram of Bi2212 as a function of hole doping. The filled symbols are the measured T_c's for the superconducting phase transition from magnetic susceptibility. The open symbols are the T^* at which the (maximum) gap seen in ARPES closes; for the $T_c = 10$K sample the symbol at 301K is a lower bound on T^*.

FIG. 13. Momentum and temperature dependence of the gap estimated from leading edge shift (see text). a) **k**-dependence of the gap along the "minimum gap locus" (see text) in the 87K T_c, 83K T_c and 10K T_c samples, measured at 14K. b) T-dependence of the (maximum) gap in a near-optimal 87K sample (circles), underdoped 83K (squares) and 10K (triangles) samples. Note smooth evolution of gap from SC to normal state for 83K sample.

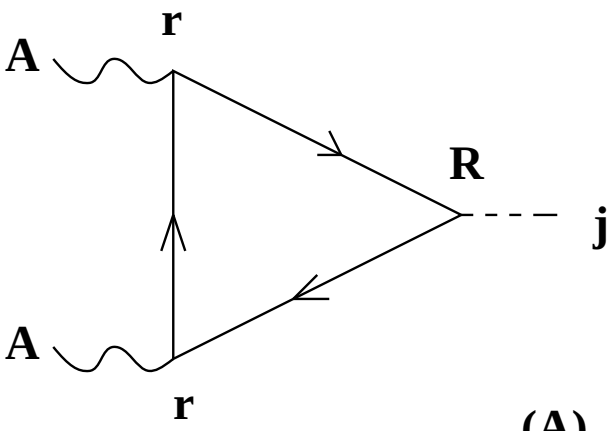

(A)

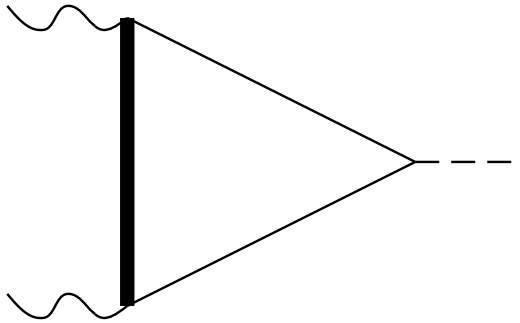

(B)

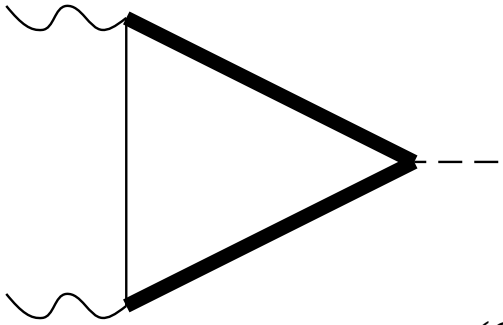

(C)

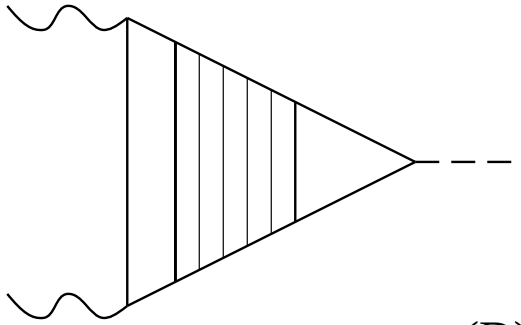

(D)

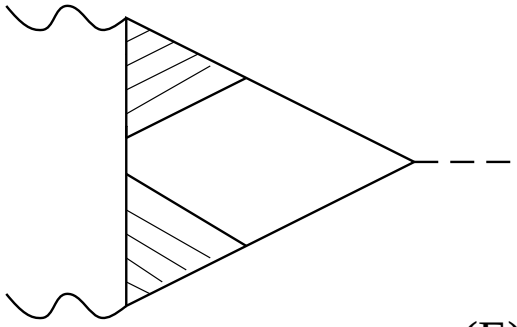

(E)

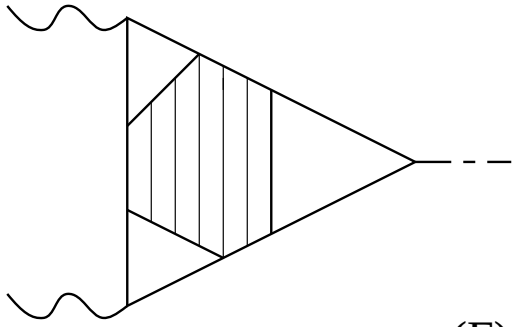

(F)